A Simple Two-Phase Route to Silver Nanoparticles/Polyaniline Structures

Marcela M. Oliveira,[†] Eryza G. Castro,[†] Carla D. Canestraro,[‡] Daniela Zanchet,[§] Daniel Ugarte,[§,||] Lucimara S. Roman,[‡] and Aldo J. G. Zarbin*[,†]

Departamento de Química, and Departamento de Física, Universidade Federal do Paraná (UFPR), CP 19081, CEP 81531−990, Curitiba-PR, Brazil, Laboratório Nacional de Luz Síncrotron (LNLS), CP 6192, CEP 13984−971, Campinas-SP, Brazil, and Instituto de Física Gleb Wataghin, UNICAMP, CP 6165, CEP 13083−970, Campinas-SP, Brazil

Received: February 9, 2006; In Final Form: July 8, 2006

Novel silver nanoparticles/polyaniline composites were obtained through a two-phase water/toluene interfacial reaction. We show that by rigorously controlling the reaction time, different structures of the nanocomposites can be obtained, such as a thin sheet of polyaniline around the silver nanoparticles or a polymer mass with nanoparticles homogeneously embedded within it. Samples were characterized by FT-IR, UV−vis−NIR and Raman spectroscopy, X-ray diffraction, cyclic voltammetry, TEM, and HRTEM. Conductivity and current−voltage characteristics of the nanocomposites were measured, and the results indicate that different properties result from the different structures in which the nanocomposites were formed.

1. Introduction

Nanocomposites formed by metal nanoparticles (NPs) dispersed in electrically conducting polymers, such as polyaniline or polypyrrole, have received much attention in the past few years.[1−13] These hybrid nanomaterials are expected to display several synergistic properties between the polymer and the metal nanoparticles, making them potential candidates for application in several fields such as catalysis,[1] biosensors,[2] memory devices,[3] sensors,[4,5] and others.[6−13] Polyaniline (PANI) is a conducting polymer of particular interest, due its high stability, low monomer cost, large conductivity range, and the different redox states that can be obtained: the fully reduced form, leucoemeraldine base (yellow); the half-oxidized form, emeraldine base (blue); and the fully oxidized form, pernigraniline (purple).[14] Besides the neutral form described earlier, polyaniline can also be doped by protonation, forming the so-called salt forms. The emeraldine salt (green) is the most conductive form of polyaniline. Due the great chromatic variation resulting from the different oxidation states of polyaniline, this polymer is commonly used as active component of electrochemical devices.[14]

The most current methods employed to incorporate inorganic nanoparticles into polymeric matrixes are based on a blend or mixture of the individual components, starting with the polymer in solution or in melt form. However, as reported by Gangopadhyay and De,[15] these approaches are not easily applicable to conducting polymers, due the fact that they are infusible and generally insoluble in common solvents. For these reasons, metal nanoparticles/conducting polymers nanocomposites have been obtained by different methods: reduction of metal salts by the already-formed polymer,[1,9,13] by using templates for growing both metal NPs and polymer into a porous structure,[16] by a photoredox mechanism,[6,7] or by electrochemical methods (through incorporation of metal NPs during the electrosynthesis of the polymer[17] or by the electrodeposition of metal NPs on preobtained conducting polymer electrodes[18]).

Recently, we developed a novel route to dodecanethiol-capped silver nanoparticles/polyaniline nanocomposite, based on a two-phase polymerization route, in which aniline was dissolved in a silver nanoparticles toluene solution that was mixed with an aqueous solution of ammonium persulfate.[19] We noticed that the polymerization took place at the water/toluene interface, and that the silver nanoparticles were carried out to the forming polymer, resulting in a polyaniline mass in which the silver nanoparticles are homogeneously dispersed. Here we show that, by simple control of certain synthesis variables for this procedure, it is possible select the structure of the nanocomposites, from a well-defined structure in which a thin sheet of polyaniline grows around each individual silver nanoparticles to silver nanoparticles incrusted into a polyaniline mass. Additionally, we show that the different structures of these nanocomposites present very specific electric behavior, which makes them suitable materials for a wide range of applications.

2. Experimental Section

The dodecanethiol-stabilized silver nanoparticles were prepared according to a previously described method,[20] based on a synthesis procedure developed by Brust el al[21] for gold nanoparticles. Typically, 3.75 mL of an aqueous $AgNO_3$ solution (0.03 mol L^{-1}) was added to 10 mL of a toluene solution containing tetraoctylammonium bromide (0.05 mol L^{-1}) to form a two-phase system. The system was maintained under vigorous stirring during 10 min to transfer the metal ion into the organic phase, which was then separated. Dodecanethiol (50.4 μL, 2.1 $\times$ 10^{-4} mol) was subsequently added to the solution with stirring, followed by a rapid injection of 3.15 mL of a 0.4 mol L^{-1} aqueous solution of $NaBH_4$ (reducing agent). The system was maintained under stirring for 3 h. The silver NPs were precipitated by the addition of excess of ethanol, subsequently isolated by centrifugation, washed with ethanol, and redissolved

* Corresponding author. Phone: +55−41−33613176. Fax: +55−41−33613186. E-mail: aldo@quimica.ufpr.br.
[†] Departamento de Química, Universidade Federal do Paraná.
[‡] Departamento de Física, Universidade Federal do Paraná.
[§] Laboratório Nacional de Luz Síncrotron.
[||] Instituto de Física Gleb Wataghin.

10.1021/jp060861f CCC: $33.50
Published on Web 08/05/2006

in toluene. The nanocrystal obtained consists of a metal core capped by thiol ligands that passivate the surface and prevent flocculation. The silver NPs displayed an average diameter of 3.8 ± 0.3 nm.

The silver nanoparticles/polyaniline nanocomposites were obtained in the following manner: 58 μL of aniline (6.29×10^{-4} mol) was mixed with 10 mL of a toluene solution of silver NPs obtained as described earlier ($\sim$0.1 g of passivated silver NPs). This solution was mixed with 30 mL of a 1 mol L^{-1} H_2SO_4 aqueous solution containing 36.8 mg of ammonium persulfate (1.48×10^{-4} mol). The two-phase system was maintained under magnetic stirring for several carefully established time intervals, at room temperature. At the selected times, the reaction was interrupted by separating the aqueous phase, adding an excess of ethanol and isolating the resulting solid by centrifugation. After the isolation step, all resulting solids were washed several times with ethanol and water and subsequently dried at 40 °C. The time during which the two-phase polymerization was allowed to proceed was defined according to the visual modifications observed in the system. After 1.5 h, the colorless aqueous solution becomes light blue and subsequently green. The green color of the aqueous solution grew more and more intense with time, and after 3 h, a highly disperse green powder was formed in the aqueous phase, with the concomitant decrease of the intensity of the brown color of the organic phase. With this in mind, we stopped the reaction at the following times: 1 h 40 min (the moment at which the aqueous phase begins to turn green), 1 h 55 min, and 3 h (a moment in which the brown color of the organic phase, which is characteristic of the silver nanoparticles, shows very low intensity. This occurrence should be an indicative that the silver NPs are carried to the aqueous phase by the former polymer). These samples will be referred to here as Ag/PANI-1, Ag/PANI-2, and Ag/PANI-3, respectively.

Pure polyaniline was also prepared following the same procedure described above. The experimental steps were carried out exactly as described for the 3-h reaction, but without the presence of silver NPs.

The X-ray diffractogram of the samples were obtained in a Shimadzu XRD-6000 diffractometer, using Cu Kα radiation, 40 kV and 40 mA at a 0.2° scan rate (in 2θ). The room-temperature measurements were performed with the samples spread on a conventional glass sample holder. Powder silicon reflections were used for 2θ calibration.

The FT-IR spectra of the samples were obtained with a Bomem MB-100 spectrophotometer in the 4000−400 cm^{-1} range with 32 scans. The samples were prepared into KBr pellets.

The Raman spectra were obtained in a Renishaw Raman Image spectrophotometer, coupled to an optical microscope that focuses the incident radiation down to an approximately 1-μm spot. A He−Ne laser (emitting at 632.8 nm) was used, with an incidence potency of 2 mW over 2000−180 cm^{-1}.

The UV−vis−NIR spectra were collected with the samples in toluene (neat Ag nanoparticles) or aqueous (neat polyaniline and nanocomposites) suspension, using air as reference, in a Scinco 1000 equipment.

TEM measurements were done in a JEOL 120 KV instrument or obtained in a JEOL 300 KV JEM 3010 microscope (HRTEM mode). The samples for observation were suspended in water and allowed to settle for 15 min. Then a drop of the supernatant dispersion was placed onto a carbon film supported by a copper grid.

To measure the cyclic voltammetry, samples were suspended in distilled water and sonificated for 15 min. This suspension was carefully transferred to the surface of a glass plate covered by a thin, transparent, and conductive film of fluorine-doped tin oxide (FTO). After water evaporation (at room temperature) a uniform and transparent film was formed inside the FTO surface, which was used as a working electrode. Measurements were performed using a Microquimica MQPG-01 potentiostat, interfaced to a PC computer. A one-compartment cell with a Pt wire as a counter electrode, a Ag/AgCl reference electrode, and a 0.1 mol L^{-1} H_2SO_4 aqueous solution as electrolyte were used. The scan speed was 50 mV s^{-1} and the potential range was from −200 to 1000 mV.

The resistivity of the samples was studied using four probe measurements. This measurement was performed using several substrates with four parallel stripes of fluorine-doped tin oxide (FTO) patterned onto glass as the electrodes. Films of each sample were deposited on top of each of these patterned substrates. The films were produced by casting 1 mL of an aqueous dispersion of the samples onto the substrate. The dispersion was prepared by using 1 mg of sample and 1.5 mL of water and then sonicated for 5 min. The films obtained by this method were continuous with morphology that was quite rough, with thickness varying from 500 to 1000 nm. The four-probe resistances were obtained by applying a constant current (a few microamperes) through the external parallel electrodes and measuring the voltage between the inner parallel electrodes.

The current−voltage characteristics of samples were measured in films that were obtained in the same way as described in the previous paragraphs. For this purpose we fabricated metal (gold or nickel) planar electrodes with a gap of a few tens of micrometers between them and deposited a film of the sample to be measured between these two electrodes. The measurements were done using both the gold and nickel electrodes, and the results were reproducible. The $I-V$ curves were measured with an HP 4141 parameter analyzer by applying several voltage runs from negative to positive bias, with good reproducibility.

3. Results and Discussion

The X-ray diffractogram of the nanocomposites (data not shown here) confirms the presence of the face-centered cubic (fcc) metallic silver on all samples, indicating that the capping dodecanethiol molecules protected the silver nanoparticles against possible oxidation by the ammonium persulfate. The polyaniline formation in all nanocomposite samples was confirmed by UV−vis, FT-IR, and Raman spectroscopy. The UV−vis spectra of the aqueous dispersion of the samples (not shown) present the characteristic polyaniline bands at $\sim$320, $\sim$415, and $\sim$700−810 nm, which are respectively attributed to $\pi-\pi^*$, polaron$-\pi^*$, and $\pi-$polaron transitions of the most conductive form of polyaniline, the emeraldine salt.[22] Figure 1 shows the FT-IR spectra of the nanocomposites, as well as the neat PANI. The spectrum of the neat polyaniline (Figure 1d) displays bands attributed to the polyaniline-emeraldine salt,[23] at 1600, 1570, 1470, 1291, 1240, 1115, and 800 cm^{-1}, confirming that this synthetic route produces the polymer in its more conductive form. The infrared spectra of the three nanocomposite samples (Figures 1, parts a, b, and c for the samples Ag/PANI-1, Ag/PANI-2, and Ag/PANI-3, respectively) are very similar and also show all the bands of polyaniline-emeraldine salt, confirming the polymer formation in all samples.

The presence of the dodecanethiol C−H stretching bands at 2955, 2923, 2872, and 2853 cm^{-1} is very noticeable on the spectra of the three nanocomposite samples. The occurrence of

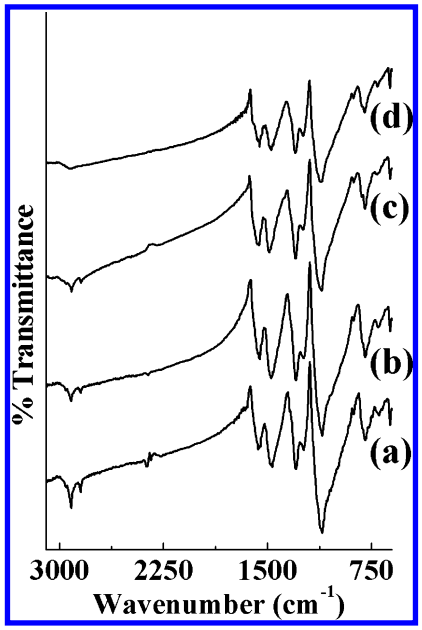

Figure 1. FT-IR spectra of the samples: (a) Ag/PANI-1, (b) Ag/PANI-2, (c) Ag/PANI-3, and (d) neat polyaniline.

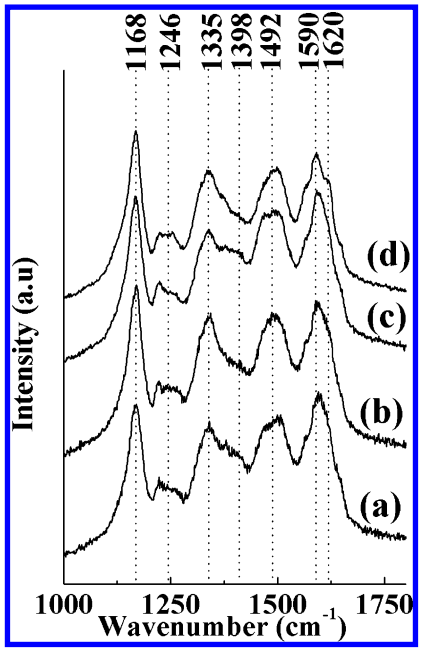

Figure 2. Raman spectra of the samples: (a) Ag/PANI-1, (b) Ag/PANI-2, (c) Ag/PANI-3 and (d) neat polyaniline.

these bands on the nanocomposite spectra is a clear signal that the dodecanethiol molecules remain on the silver NPs surface after the polymerization step. Also, it is possible to note that the intensity of these bands, in relation to the polyaniline band at 1115 cm^{-1}, is reduced from sample Ag/PANI-1 to Ag/PANI-2 to Ag/PANI-3, which can be indicative that the relative amount of polymer on the sample grows during the reaction time.

Figure 2 shows the resonance Raman spectra of the nanocomposites and of the neat polyaniline. These spectra were collected with the 632.8-nm laser, the frequency of which is coincident with the visible absorption band assigned to the radical cation segment of the polyaniline-emeraldine salt. Therefore, as expected, the quinoid and semiquinoid Raman bands are very salient in the spectra. As we can see in Figure 2, all the spectra are very similar and are in agreement with previously described spectra of pure emeraldine salt,[24,25] with the following main bands: ~1620 cm^{-1} (ν C−C of aromatic ring), 1590 cm^{-1} (ν C═C of the quinoid rings), ~1492 cm^{-1} (ν C═N of the quinoid diimina units), ~1398 cm^{-1} (due the (ν $C-N^+$ polaron), ~1335 cm^{-1} (ν C−N radical cation), ~1246 cm^{-1} (ν C−N benzene diamine units), and ~1168 cm^{-1} (ν C−H bending of the quinoid rings).

Figure 3 shows the TEM images of the samples. Parts A and B of Figure 3 show the neat Ag NPs and polyaniline, respectively. The neat Ag NPs have a medium diameter of 3.8 nm and a very narrow size distribution, as reported previously.[20] The neat polyaniline obtained by this route presents some fibrous regions, as observed in Figure 3B. The images of sample Ag/PANI-1, representative of the whole sample, are illustrated in Figure 3C,D. This sample is formed by a lot of well-separated silver nanoparticles surrounded by an asymmetric polymer shell (one individual arrangement of the polymer around the silver nanoparticle can be seen on the detail of the Figure 3D). No regions containing neat polymer or neat silver NPs were detected from the analysis of several TEM images collected in different portions of the sample, indicating that the sample presents a good uniformity. It is interesting to note that, in all structures, the metallic particle and the polymeric sheet around it were not concentric at all, and the polyaniline presents an asymmetric tail. This feature can be related to the two-phase system in which the polymerization took place, as will be discussed later.

On the images of sample Ag/PANI-2 (in which the system remains reacting for 1 h 55 min) shown in Figure 3E,F, it is possible to observe that, besides the morphologies observed on the first sample, there are several small agglomerates containing two, three, or more particles connected by polymer fragments (marked by arrows in Figure 3E,F and pointed out in the detail of Figure 3F), which indicate that the silver/polymer arrangements formed on the beginning of the process (1 h 40 min, sample Ag/PANI-1) start an agglomeration process if the system remains under reaction. The final sample, Ag/PANI-3 is formed by the metal nanoparticles homogeneously and well-dispersed in a polymer mass, as can be seen in Figure 3G−I. The inset in Figure 3G represents the electron diffraction pattern of a selected area of the Ag/PANI-3 sample, and the diffraction rings should be indexed to fcc silver metal. Figure 3H shows a dark-field image of the corresponding bright-field area showed in Figure 3G. The crystalline nature of the embedded particles is clear from this image. Figure 3H represents an HRTEM image of this sample, in which it is possible to see, in detail, a single silver nanoparticle. The lattice fringes of $d = 0.235$ nm can be attributed to the (111) planes of the fcc metallic silver, which corroborate the XRD and electron diffraction data and show that the precursor silver NPs were not oxidized during the aniline polymerization.

The results presented until now show that it is possible to prepare different samples consisting of silver nanoparticles/polyaniline composites by using exactly the same reactional system and changing just the time in which the reaction was conducted. It is important to notice that all the possible morphologies showed on the pictures of Figure 3 can be obtained as a final and very stable product, which means that once the reaction was stopped at the desired time, the obtained product remains exactly with the morphology in which it was formed.

The sequence of the TEM images presented in Figure 3 is highly elucidative in relation to the steps in which the nanocomposites are formed by this route. On the basis of these images, we propose the following mechanism, schematically illustrated in Figure 4: since the silver nanoparticles were homogeneously mixed with aniline in the toluene solution, they

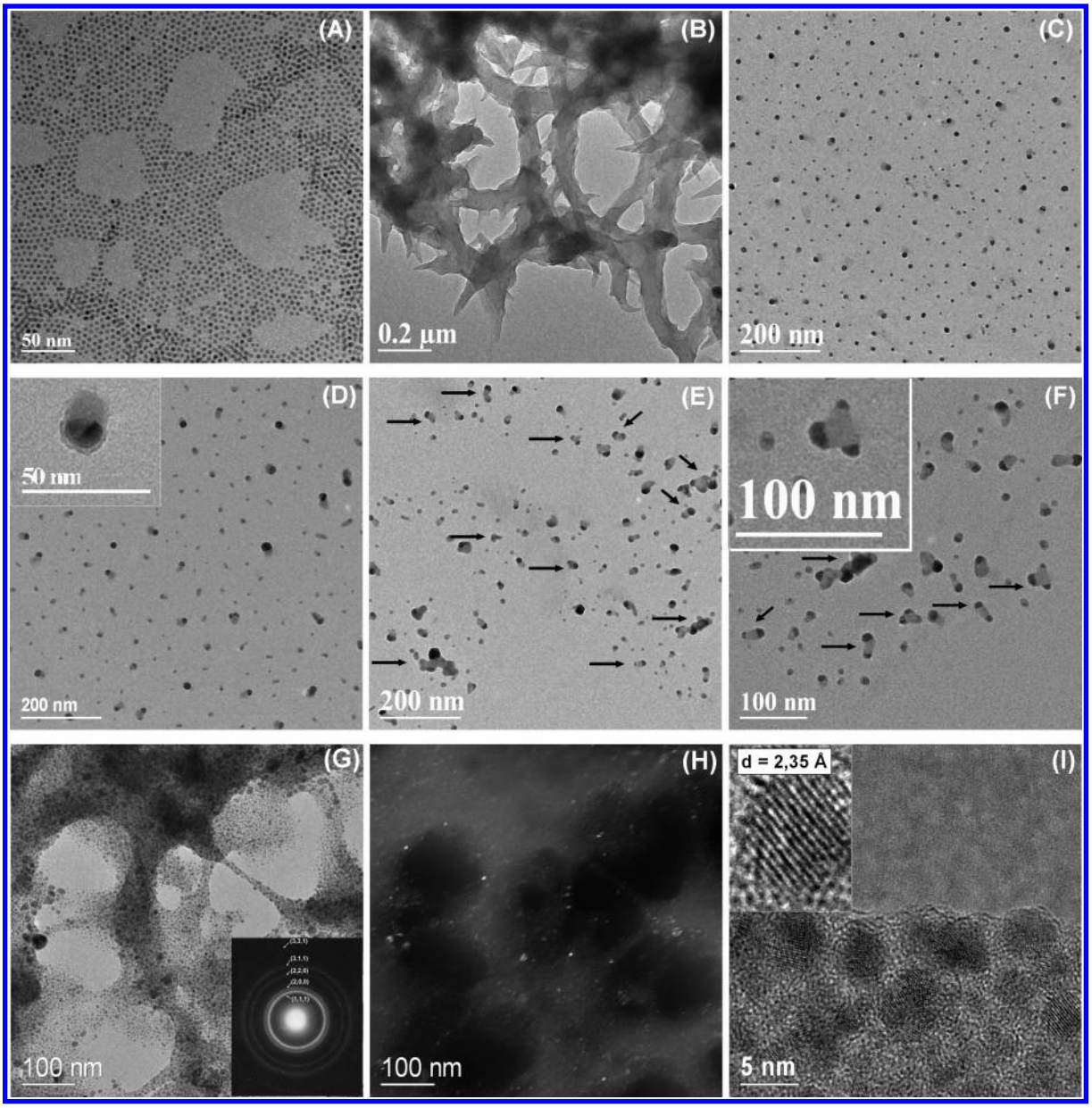

Figure 3. TEM image of the samples: (A) neat Ag nanoparticles, (B) neat polyaniline, (C and D) Ag/PANI-1, (E and F) Ag/PANI-2, (G) Ag/PANI-3, (H) dark-field image corresponding to the bright-field area presented in part G, and (I) high-resolution image of Ag/PANI-3. The detail in part D shows a single silver nanoparticle encapsulated by a polyaniline shell. The arrows in part E and the inset in part F show small agglomerates of particles linked by polymer fragments (see the text). The inset in part G corresponds to a electron diffraction indexed to the fcc silver metal. The inset in part I shows a HRTEM of a silver particle embedded in the polyaniline mass of sample Ag/PANI-3.

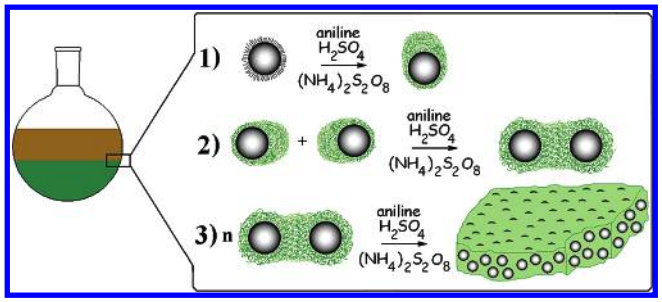

Figure 4. Proposed mechanism for the silver nanoparticles/polyaniline nanocomposite formation: (1) silver NPs act as nucleation centers for polyaniline growth; (2) the forming polymer grows from the polymer initially formed on the silver nanoparticles, connecting two or more nanoparticles; (3) by repeating steps 1 and 2, a large polymer mass containing silver nanoparticles embedded within it is formed.

could be acting as nucleation centers for the polymerization. Once the polymerization occurs at the interface of the organic (containing the aniline and the silver NPs) and aqueous (containing the oxidizing) phase, the polymer grows initially around the silver NPs, drawing it to the aqueous phase and forming the asymmetric thin sheet of polyaniline around the silver nanoparticles observed in sample Ag/PANI-1 (remember that this sample corresponds to the moment at which the aqueous phase starts to turns green, the PANI color). This occurrence is sketched in step 1 of Figure 4. As the reaction continues, the excess of aniline present at the interface begins to polymerize, growing around the formed polymer/silver structures and promoting the agglomeration observed in Figure 3E,F for sample Ag/PANI-2 (as sketched in step 2 of Figure 4). By a repetition of this process, the final material should be exactly as observed in the images of sample Ag/PANI-3 (Figure 3E,F); in other words, the forming polyaniline continues to grow around the agglomerates, resulting in a polymer mass with the nanoparticles homogeneously embedded within it (step 3, Figure 4).

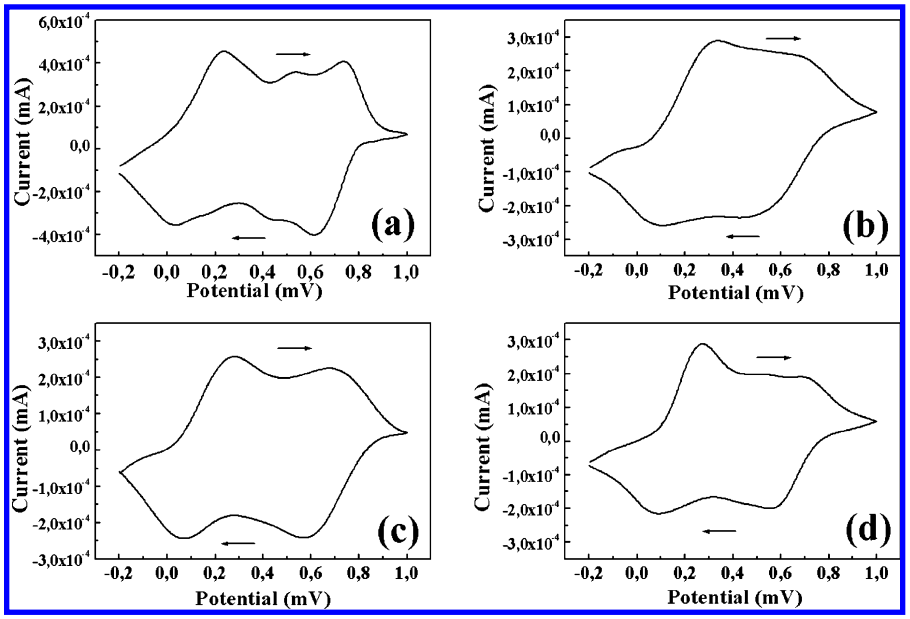

Figure 5. Cyclic voltammogram of the samples: (a) neat polyaniline, (b) Ag/PANI-1, (c) Ag/PANI-2, and (d) Ag/PANI-3. Electrolyte = H_2SO_4 (0.1 mol L^{-1}), reference electrode = Ag/AgCl, counter-electrode = Pt wire, scan velocity = 50 mV s^{-1}.

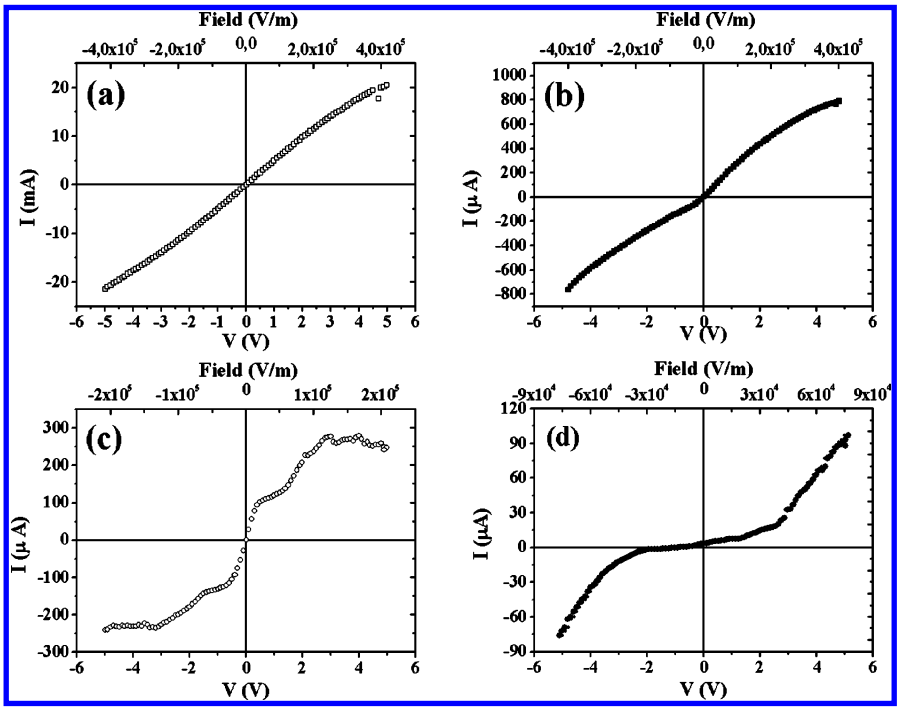

Figure 6. *I*−*V* curves of the samples: (a) neat Ag nanoparticles, (b) neat polyaniline, (c) Ag/PANI-1, and (d) Ag/PANI-3.

To verify if the different structures of these Ag/PANI nanocomposites give rise to different properties, we investigated the electrochemical and electric behavior of the bulk samples. The cyclic voltammograms of all samples (Figure 5) show two well-defined reversible redox processes characteristic of polyaniline,[26] confirming that the polymer presents electroactivity. During voltammogram acquisition, the typical polyaniline color changes are observed, showing that the materials display electrochromism. The neat polyaniline voltammogram (Figure 5a) displays, in addition to the two redox peaks, an intermediary redox process usually observed for chemically polymerized polyaniline and attributed to ortho-coupling or cross-linking of the polymer.[26] This intermediary redox process was not observed on the voltammograms of samples Ag/PANI-1 and Ag/PANI-2 and appears for sample Ag/PANI-3, which can be indicative that the process of ortho-coupling or cross-linking in the polymer chains starts after the initial polymer was formed in samples Ag/PANI-1 and Ag/PANI-2, concomitantly with the appearance of the polymeric mass, which supports our model for nanocomposites formation. Also, two other important information were obtained from the voltammograms of the nanocomposites: (i) there are no signals attributed to the neat silver nanoparticles (silver oxidation or dodecanethiol desorption), at least at the scan velocity used in these experiments, confirming that, in fact, the nanoparticles are fully protected by the polymer; (ii) the separation between the two main redox peaks of the polymer is less for the Ag/PANI-1 sample (Figure 5b) and continuously increases for Ag/PANI-2, Ag/PANI-3, and neat polyaniline (the separation between the two main oxidation peaks is 340, 410, 450, and 505 mV for samples Ag/PANI-1, Ag/PANI-2, Ag/PANI-3, and neat PANI, respectively). An approximation of the two redox peaks, as well as a poor

definition between the two peaks (as observed on the voltammogram of the Ag/PANI-1 sample, Figure 5b), was observed for some polyaniline/metal particle nanocomposites[27,28] and has been attributed to a strong interaction between the polymer and the metal nanoparticles. This attribution agrees with what is expected for our system, given that the polyaniline/Ag NPs interaction is supposed to be stronger for the Ag/PANI-1 sample, due the higher proximity between the polymer shell and the silver particle, diminishing as the amount of polymer increases in the sample.

The resistivity of the bulk samples was studied using four-probe measurements. Four-probe measurements are indicated for obtaining the resistivity (or conductivity) of thin films, without interference from the contact resistance between the electrode and the material composing the active layer. The results for the sample conductivities were as follows: 0.4 S cm^{-1} (neat polyaniline), 2.3 S cm^{-1} (Ag/PANI-1), and 1.7 S cm^{-1} (Ag/PANI-3). As expected, the conductivity of the PANI increases by 4−5 times upon the insertion of silver nanoparticles, and both the nanocomposite materials present even higher conductivity. Also, the nanocomposite in which the polymer growth is around the individual silver particles (Ag/PANI-1) displays higher conductivity than the nanocomposite formed by the nanoparticles embedded within the polymer. This could be related to the more effective metal/polymer interactions achieved by this sample, as suggested by the cyclic voltammogram results discussed earlier.

The current−voltage characteristics obtained from the neat Ag nanoparticles, neat PANI, Ag/PANI-1, and Ag/PANI-3 samples are shown in Figure 6.

From Figure 6 it is possible to clearly see that the electrical properties of the two nanocomposites are very different from those observed for their individual component (Ag NPs and PANI), confirming the occurrence of true nanocomposites (with synergistic properties between the components that are not attributed to either individual component). Also, it is clear from the $I-V$ curves that the properties of the two Ag/PANI nanocomposites are entirely different between them, confirming the importance of process control on the nanocomposite structure in order to obtain different and selected properties. The $I-V$ characteristic curves for neat Ag nanoparticles and neat PANI (Figure 6, parts a and b, respectively) displayed ohmic behavior. The Ag/PANI-3 curves (Figure 6d) displayed a diode-like curve for which the dependence of current on voltage can be divided into three regions: the first region from 0 to 1.2 V displays linear behavior; a transition region, from 1.2 to 2.5 V; and the third region, above 2.5 V, where the current depends quadratically on voltage.

The Ag/PANI-1 sample (Figure 6c) displays quite different $I-V$ characteristics, marked by the occurrence of two plateaus, one initiating around 0.5 V and other initiating at 3 V. The dependence of current on voltage below 0.5 V is sublinear, with a plateau between 0.5 and 1.5 V. The current varies linearly with the voltage between 1.5 and 3V, reaching another plateau, a saturation of the current with increasing applied bias, reaching an almost constant value. The current remains constant even for higher applied voltages.

At this time it is not possible to propose mechanisms explaining the origin of the events associated with the different responses observed on the $I-V$ curves of the nanocomposites samples. It is clear to us, however, that they are associated with charge transfer between the two components (polymer and metal NP) and are strongly influenced by the interfaces between these components. Theoretical calculations and new experiments are currently in progress in order to clarify this point.

4. Conclusions

In summary, we have reported a very simple route to production of novel silver nanoparticles/polyaniline nanocomposites, in which different morphologies can be achieved by rigorously controlling the synthesis procedure. To our knowledge, this is the first report on a synthetic route in which different silver nanoparticles/polyaniline structures could be obtained as stable materials in the same reaction system by changing just the time in which the reaction was conducted. On the basis of the obtained results, we suggest a mechanism for the nanocomposites formation. Besides the strategy to control the morphology of the final materials, this work shows very important results concerning the electrical and electrochemical behavior of the different samples. These properties were dependent on the kind of morphology adopted by the nanocomposite, emphasizing the fundamental importance of controlling synthesis parameters (in order to control the morphology of the final material). We believe that the synthesis approach presented in this paper can be extended to other nanoparticles/polymers pairs and should become a very effective route to different nanocomposite materials. Efforts in this direction are currently being done in our laboratory.

Acknowledgment. The authors would like to thank the Brazilian agencies CNPq, CT-ENERG/CNPq, and Rede de Materiais Nanoestruturados for funding, Centro de Microscopia Eletrônica-UFPR and Laboratório de Microscopia Eletrônica-LNLS for the TEM images, and Prof. Ney Mattoso (DF-UFPR) for the dark-field TEM images. M.M.O. and C.D.C. thank CAPES for the fellowship.

References and Notes

(1) O'Mullane, A. P.; Dale, S. E.; Macpherson, J. V.; Unwin, P. R. *Chem. Commun*. **2004**, 1606−1607.
(2) Tian, S.; Liu, J.; Zhu, T.; Knoll, W. *Chem. Mater*. **2004**, *16*, 4103−4108.
(3) Tseng, R. J.; Huang, J.; Ouyang, J.; Kaner, R. B.; Yang, Y. *Nano Lett*. **2005**, *5*, 1077−1080.
(4) Sharma, S.; Nirkhe, C.; Pethkar, S.; Athawale, A. A. *Sens. Actuators, B* **2002**, *85*, 131−136.
(5) Majumdar, G.; Goswami, M.; Sarma, T. K.; Paul, A.; Chattopadhyay, A. *Langmuir* **2005**, *21*, 1663−1667.
(6) Khanna, P. K.; Singh, N.; Charan, S.; Viswanath, K. *Mater. Chem. Phys.* **2005**, *92*, 214−219.
(7) Barros, R. A.; Azevedo, W. M.; Aguiar, F. M. *Mater. Charact*. **2003**, *50*, 131−134.
(8) Sarma, T. K.; Chattopadhyay, A. *Langmuir* **2004**, *20*, 4733−4737.
(9) Wang, J.; Neoh, K. G.; Kang, E. T. *J. Colloid Interface Sci*. **2001**, *239*, 78−86.
(10) Breimer, M. A.; Yevgeny, G.; Sy, S.; Sadik, O. A. *Nano Lett*. **2001**, *1*, 305−308.
(11) Kumar, T.; Chattopadhyay, A. *J. Phys. Chem. A* **2004**, *108*, 7838−7842.
(12) Sivakumar, M.; Gedanken, A. *Synth. Met*. **2005**, *148*, 301−306.
(13) Zhou, Y.; Itoh, H.; Uemura, T.; Naka, K.; Chujo, Y. *Langmuir* **2002**, *18*, 277−283.
(14) Genies, E. M.; Boyle, A.; Lapkowski, M.; Tsintavis, C. *Synth. Met*. **1990**, *36*, 139−182.
(15) Gangopadhyay, R.; De, A. *Chem. Mater*. **2000**, *12*, 608−622.
(16) Marinakos, S. M.; Shultz, D. A.; Feldheim, D. L. *Adv. Mater*. **1999**, *11*, 34−37.
(17) Vork, F. T. A.; Janssen, L. J. J.; Barendrecht, E. *Electrochim. Acta* **1986**, *31*, 1579−1575.
(18) Holdcroft, S.; Funt, B. L. *J. Electroanal. Chem.* **1988**, *240*, 89−103.
(19) Oliveira, M. M.; Zanchet, D.; Ugarte, D.; Zarbin, A. J. G. *Prog. Colloid Polym. Sci.* **2004**, *128*, 126−130.
(20) Oliveira, M. M.; Zanchet, D.; Ugarte, D.; Zarbin, A. J. G. *J. Colloid Interface Sci*. **2005**, *292*, 429−435.

(21) Brust, M.; Walker, M.; Bethell, D.; Schiffrin, D. J.; Whyman, R. *J. Chem. Soc. Chem. Commun.* **1994**, *7*, 801−802.
(22) Xia Y.; Wiesinger M.; MacDiarmid, A. G. *Chem. Mater.* **1995**, *7*, 443−445.
(23) Furukawa, Y.; Ueda, F.; Hyodo, Y.; Harada, I.; Nakajima, T.; Kawagoe, T. *Macromolecules* **1988**, *21*, 1297−1305.
(24) Quillard, S.; Berrada, K.; Lovarn, G.; Lefrant, S.; Lapkowiski, M.; Pron, A. *New J. Chem.* **1995**, *19*, 365−374.
(25) Pereira da Silva, J. E.; Temperini, M. L. A.; Torresi, S. I. C. *Electrochim. Acta* **1999**, *44*, 1887−1891.
(26) Genies, E. M.; Lapkowski, M.; Penneau, J. F. *J. Electroanal. Chem.* **1988**, *249*, 97−107.
(27) Zimmer, A. M.; Bertholdo, R.; Grassi, M. T.; Zarbin, A. J. G.; Mascaro, L. H. *Electrochem. Commun.* **2003**, *5*, 983−988.
(28) Delime, F.; Leger, J. M.; Lamy, C. *J. Appl. Electrochem.* **1988**, *28*, 27−35.